UC Berkeley
UC Berkeley Previously Published Works

Title

Quantitative Assessment of Myocardial Ischemia With Positron Emission Tomography

Permalink

Journal

ISSN

Authors

Sohn, Jae Ho
Behr, Spencer C
Pampaloni, Miguel Hernandez
et al.

Publication Date

2023-07-01

DOI

Peer reviewed

Quantitative assessment of myocardial ischemia with PET

Jae Ho Sohn, MD, MS[*], **Spencer C. Behr, MD**[*], **Pampaloni Miguel Hernandez, MD, PhD**[*], **Youngho Seo, PhD**[*,†,‡]

[*]Department of Radiology and Biomedical Imaging, University of California, San Francisco, CA

[†]Department of Radiation Oncology, University of California, San Francisco, CA

[‡]UC Berkeley-UCSF Graduate Program in Bioengineering, Berkeley and San Francisco, CA

Abstract

Recent advances in PET technology and reconstruction techniques have now made quantitative assessment using cardiac positron emission tomography (PET) readily available in most cardiac PET imaging centers. Multiple PET myocardial perfusion imaging (MPI) radiopharmaceuticals are available for quantitative examination of myocardial ischemia, with each having distinct convenience and accuracy profile. Important properties of these radiopharmaceuticals (^{15}O-water, ^{13}N-ammonia, ^{82}Rb, ^{11}C-acetate, and ^{18}F-flurpiridaz) including radionuclide half-life, mean positron range in tissue, and the relationship between kinetic parameters and myocardial blood flow (MBF) are presented. Absolute quantification of myocardial blood flow (MBF) requires PET MPI to be performed with protocols that allow the generation of dynamic multiframes of reconstructed data. Using a tissue compartment model, the rate constant that governs the rate of PET MPI radiopharmaceutical extraction from blood plasma to myocardial tissue is calculated. Then, this rate constant (K_1) is converted to MBF using an established extraction formula for each radiopharmaceutical. Since most of the modern PET scanners acquire the data only in list-mode, techniques of processing the list-mode data into dynamic multiframes are also reviewed. Finally, the impact of modern PET technologies such as PET/CT, PET/MR, total-body PET, machine learning/deep learning on comprehensive and quantitative assessment of myocardial ischemia is briefly described in this review.

Keywords

PET; myocardial perfusion imaging; quantitative PET; dynamic PET; kinetic modeling; extraction fraction; myocardial ischemia; myocardial blood flow; MBF; coronary flow reserve; CFR; machine learning; deep learning

Introduction

Myocardial ischemia typically occurs when there is a disbalance between supply and demand of oxygen to a specific region, which most often is a consequence of a chronic or acute flow-limiting stenosis through the epicardial coronary vessels. Myocardial ischemia

Correspondence to: Youngho Seo, PhD, UCSF Physics Research Laboratory,185 Berry St, Ste 350, San Francisco, CA 94143-0946, USA, Phone: (415)353-9464; Fax: (415)353-9423; youngho.seo@ucsf.edu.

induces local hypoxia that could lead to tissue death (i.e., myocardial infarction) unless successfully intervened in a timely fashion. The accurate identification of the jeopardized myocardial areas is of paramount importance for adequate restoration of the blood flow.[1–3]

Noninvasive assessment of myocardial ischemia is best performed by cardiac imaging modalities such as single photon emission computed tomography (SPECT), positron emission tomography (PET), cardiac magnetic resonance imaging (CMR), x-ray computed tomography (CT), and echocardiography. A recently published consensus statement by the Quantitative Cardiac Imaging Study Group, derived from a European quantitative cardiac imaging meeting, summarizes the advantages and disadvantages of each imaging technique for the assessment of myocardial ischemia.[4]

Of these imaging modalities, this review focuses on quantitative cardiac PET myocardial perfusion imaging (MPI) for assessment of myocardial ischemia by presenting its capabilities, how it is performed, and how the image data are interpreted. Furthermore, we will discuss the choice of relevant radiopharmaceuticals, relevant PET imaging technology developments, image formation process, technological advances in image generation to improve the image quality and quantitation, and quantification techniques in PET MPI. A particular emphasis is placed on how to ensure consistency with quantification in PET MPI, how information from quantitative cardiac PET is produced from modeling, and how to choose the most appropriate cardiac PET perfusion radiopharmaceutical. Latest technological advances such as time-of-flight (TOF) PET data acquisition and processing as well as machine learning approaches are discussed in relation to quantitative PET MPI.

Advantages and disadvantages of cardiac PET

Any clinically accepted imaging modality for the assessment of myocardial ischemia has distinct advantages and disadvantages.[4–8] One of the most recognized advantages for cardiac PET is quantification of myocardial blood flow (MBF). In addition, the MBFs calculated for stress and rest states are bases for calculating coronary flow reserve (CFR), which is defined as MBF_{stress}/MBF_{rest}. In particular, when cardiac PET is performed dynamically using ^{15}O-H_2O (i.e., ^{15}O-water) as its radiopharmaceutical, a simple kinetic model can easily quantify MBF as an influx rate constant, K_1 (mL min^{-1} g^{-1}). Since ^{15}O-water is an ideal, freely diffusible radioactive molecule, the rate of this molecule's transition from the blood plasma to the myocardial tissue represents the true MBF. Hence, the tracer uptake pattern, as represented in the reconstructed images, of ^{15}O-water cardiac PET represents the true myocardial perfusion map.

However, ^{15}O has a very short physical half-life (122.24 seconds), which makes it challenging for daily clinical workflows at most facilities.[9] Fortunately, several other radiopharmaceuticals are readily available for PET MPI, though with some physiological drawbacks.[9,10] Namely, none other than ^{15}O-water provides the true linear relationship between the uptake and blood flow, also known as the extraction fraction. Basically, all other currently available cardiac PET radiopharmaceuticals and contrast agents are metabolically trapped in the intracellular space,[10] and the extraction typically becomes nonlinear at high myocardial blood flow rates.

Therefore, it is important to understand the characteristics of each radiopharmaceutical that can be used for clinical PET MPI. Of particular interest for this review are quantitative aspects of these radiopharmaceuticals as highlighted next.

Radiopharmaceuticals for quantitative cardiac PET

Extraction fraction is a relationship that is established between the uptake of radiopharmaceutical and regional blood flow. For ^{15}O-water, this relationship is linear, one-to-one, meaning that the higher the uptake is, the higher the myocardial blood flow. However, there are some notable challenges for ^{15}O-water usage in PET MPI. First, [15]O has an extremely short physical half-life (122.24 seconds) so that the transport distance must be very short between the ^{15}O-water production site and the ^{15}O-water dispenser to the cardiac PET scan. This requirement implies that a facility needs not only an on-site cyclotron and a radiopharmacy laboratory that can clinically dispense the labeled product, but also a logistical solution for a streamlined transport of the radiopharmaceutical from the production site to the injection site (i.e., in the PET scanner room). Another challenge for ^{15}O-water is that [15]O has a relatively long positron range (mean range in water ~3.0 mm), a characteristic different for each positron-emitting radionuclide. A large positron range results in degradation of image spatial resolution. For this reason, reconstructed ^{15}O-water PET images do not possess the same image quality as ^{18}F-based radiopharmaceuticals. In fact, ^{18}F has the shortest positron range (mean range in water ~0.6 mm) among those positron emitters used in human subjects.[11] Additionally, water is a freely diffusible molecule with no intracellular trapping. Hence, there is basically no prolonged accumulation of ^{15}O-water in myocardium, further degrading the image quality driven by low contrast.

For these reasons among others, much effort has been made to improve the accuracy of myocardial blood flow quantification with alternative radiopharmaceuticals. The list of suitable PET radiopharmaceuticals for myocardial perfusion imaging includes [82]Rb, ^{13}N-NH$_3$ (i.e., ^{13}N-ammonia), ^{11}C-acetate, and ^{18}F-flurpiridaz[12]; all of which have a wealth of literature detailing how to perform perfusion imaging and quantify blood flow using appropriate kinetic modeling. Although each radiopharmaceutical has distinct advantages as a PET MPI agent, the ultimate choice of a radiopharmaceutical primarily depends on several practical factors including the US Food and Drug Administration (FDA) approval status or equivalent regulatory approval in other countries, reimbursement mechanism from insurance providers, onsite cyclotron and radiopharmacy availability as well as the cost of maintaining a [82]Sr/[82]Rb generator system for producing [82]Rb.

Table 1 summarizes several key aspects for ^{15}O-water, [82]Rb, ^{13}N-ammonia, ^{11}C-acetate, and ^{18}F-flurpiridaz, which can all be used for the assessment of myocardial perfusion. Figure 1 shows differences in the linearity between uptake and myocardial blood flow for ^{15}O-water, ^{13}N-ammonia, ^{18}F-flurpiridaz, and other relevant radiopharmaceuticals, illustrating the ideal property of ^{15}O-water, followed by those of ^{18}F-flurpiridaz and ^{13}N-ammonia for the task of MBF quantification.

$^{15}O\text{-}H_2O$ ($^{15}O\text{-water}$)

^{15}O-water's characteristics have been described extensively already. It is technically a radioactive water molecule. Its perfusion in the myocardium is a true representation of perfusion and blood flow. ^{15}O-water does not enter further metabolic processes, and there is no binding to the tissue directly. This eases computational modeling to derive myocardial blood flow (MBF). MBF is computed from dynamic ^{15}O-water PET data as a rate constant in the one-tissue compartment model, which is the flow rate per mass (mL min^{-1} g^{-1}) from the arterial blood pool to the water-perfusable myocardial tissue. Similarly, ^{15}O-water PET can be used for measuring blood flow in all other parts of the human body including the brain and tumors.[13–16]

^{82}Rb ($^{82}RbCl$)

Rubidium-82, $^{82}RbCl$, or just ^{82}Rb is available through an $^{82}Sr/^{82}Rb$ generator and is the most commonly used PET MPI agent due its commercial availability. The short half-life of ^{82}Rb (1.273 minutes or 76.4 seconds) allows for repeated or combined stress-rest at short intervals. Since the generator is small and can be stationed within the PET scanner room, there is no need to resolve a logistical issue of transportation between the production site and the scanner room.

Rb-82 acts is a potassium analog and acts as a metabolic analogue as it is taken up via the sodium-potassium adenosine triphosphatase pump (ATP).[17–19] Quantitatively, the extraction of ^{82}Rb is inversely and nonlinearly proportional to the blood flow especially at high flow values (>2.5 mL min-1 g),[20] which makes ^{82}Rb challenging to quantify high MBF. Fortunately, in most cases, ^{82}Rb PET data can be used to reliably quantify MBF (Fig. 2) since the flow values seldom exceed the inverse relationship portion of the extraction curve, and several validation and reproducibility studies have confirmed its utility in quantitative imaging.[21–23]

It is not possible to describe cardiac PET without discussing $^{82}Rb/^{82}Sr$ generators. These generators are commercially available so that a cardiac PET imaging center can purchase and routinely incorporate it into their clinical practice. Rb-82 produced from the commercial generator does not require any further reaction before administration to the patient unlike other PET MPI radiopharmaceuticals that require production of radionuclides (i.e., ^{15}O, ^{13}N, ^{11}C, and ^{18}F) followed by chemical reaction to make the final labeled product ready for administration. Hence, the value of this generator for reliable cardiac PET imaging center operation is enormous since production of other presumably better radiopharmaceuticals, in terms of quantitative aspects, is sometimes less reliable.

For the quantitative aspect, ^{82}Rb has some challenges. Although ^{82}Rb can produce reliable and consistent quantification such as MBF in most cases with its extraction fraction corrected using an empirically derived formula, the suboptimal linearity of MBF to the ^{82}Rb uptake at high MBF values, and the suboptimal image quality due to a large positron range (mean range in water ~7.1 mm) compared to radiopharmaceuticals labeled with other positron emitters, specifically, ^{13}N and ^{18}F, lead to the demand of improved and reliable PET perfusion imaging developments. Finally, with more clinically accepted software for

dynamic cardiac PET image processing being available, building quantitation of [82]Rb-PET studies for MBF and coronary flow reserve (CFR) into a clinical cardiac PET program needs to be carefully assessed.[24]

[13]N-NH$_3$ (^{13}N-ammonia)

[13]N-ammonia is favored by many for quantification of MBF and CFR because it overcomes several of ^{15}O-water's shortcomings due to its longer half-life, improved retention in myocardium, and a shorter positron range. ^{13}N-ammonia is similar to ^{15}O-water in terms of linearity between uptake and myocardial blood flow except for very high flow values.[9] This property simplifies the calculation of MBF from K_1 rate constant calculated from the simple one-tissue compartment model or two-tissue compartment model.[25] The first-pass extraction of ^{13}N-ammonia is very high at 80%, resulting in the high linearity between MBF and uptake.[26,27] When ^{13}N-ammonia enters myocyte, it is eventually metabolically trapped by incorporating into the glutamine pool.[28,29] For static image acquisition, these properties actually help to increase the image contrast of mapping the myocardial perfusion distribution. Figure 3 shows excellent image qualities for ^{13}N-ammonia PET MPI. Different PET acquisition types (2D vs. 3D) and reconstruction algorithms further improve the image quality of ^{13}N-ammonia and other PET reconstructed images.

However, the availability of ^{13}N-ammonia, similar to that of ^{15}O-water, suffers from its short half-life (9.965 minutes), requiring an onsite or nearby cyclotron facility that can transport the labeled ^{13}N-ammonia to the PET scanner room promptly. However, in comparison to ^{15}O-water, its shorter positron range (mean range in water ~1.8 mm) and its longer half-life (9.965 minutes vs. 2.04 minutes) allow easier handling of radiopharmaceutical before injection and better image quality that leads to improved delineation of myocardium, which in turn improves automated detection of myocardium in clinical software for quantification.[30] Importantly, most of clinically accepted MBF quantification software packages consider ^{13}N-ammonia as a reference standard (e.g., ^{11}C-acetate data quantified with ^{13}N-ammonia values as a reference as in Fig. 4), and validation and reproducibility have been extensively tested.[31,32]

[11]C-acetate

Although there is little dedicated use of ^{11}C-acetate in myocardial perfusion imaging, the high first-pass extraction of ^{11}C-acetate provides an excellent means of studying myocardial perfusion (Fig. 4).[33–35] With other interests of using ^{11}C-acetate such as myocardial oxygen consumption and cancer imaging, ^{11}C-acetate is a versatile PET imaging agent that possesses favorable properties for quantitative cardiac PET imaging. A main potential disadvantage of ^{11}C-acetate stems from the fact that the influx of ^{11}C-acetate into cardiomyocytes during ongoing myocardial ischemia may be replaced by the more rapid utilization of glucose-based molecules, the favored substrate in ischemic conditions, as a consequence of the metabolic shifting of the myocardium.

The half-life of [11]C (20.334 minutes) and its relatively short positron range (mean range in water ~1.2 mm) also make ^{11}C-acetate an excellent imaging agent to ease the process of quantitative PET imaging.

^{18}F-flurpiridaz

There have been numerous developments towards an ideal PET MPI agent using ^{18}F. ^{18}F-based radiopharmaceuticals enjoy the best-in-class positron range (the shortest) resulting in excellent image spatial resolution once reconstructed, and favorable half-life (1.8295 hours) allows for convenient production and distribution. Unfortunately, very few ^{18}F-based radiopharmaceuticals for PET MPI have advanced to phased clinical trials required for regulatory approval. ^{18}F-flurpiridaz, derived from pyridazinone, that binds to mitochondrial complex-1, is one that has advanced to phased clinical trials.[36–41] Its status for FDA or other equivalent regulatory approval in other countries is still not final though. Their second Phase III clinical trial is currently ongoing (NCT03354273) as of mid-2020. The first Phase III trial for ^{18}F-flurpiridaz did not meet all study goals, necessitating the second Phase III trial. Many in the field await the final result of this trial.

Regardless of its approval status, ^{18}F-flurpiridaz is an outstanding imaging agent from both qualitative and quantitative perspectives (Fig. 5), garnering widespread attention from the field. The first-pass extraction for ^{18}F-flurpiridaz is even better than ^{13}N-ammonia, closely aligned with the linearity of ^{15}O-water between MBF and uptake. The best-in-class spatial resolution and image contrast over ^{15}O-water and all other PET MPI radiopharmaceuticals could be capitalized into more robust and reproducible myocardial segmentation and precise regional MBF and CFR quantification.

PET technologies for quantitative myocardial perfusion imaging

The original clinical PET technology was a standalone PET that did not incorporate any transmission source or CT for attenuation correction. When the significance of attenuation and scatter corrections became increasingly evident, commercial PET scanners began to incorporate built-in transmission sources such as rotating ^{68}Ge rods. Quantitative PET imaging of any part of the body, especially the heart, greatly depends on the accuracy of attenuation and scatter corrections.

The advent of PET/CT solved many problems of a standalone PET, including slow speed of transmission scans and a frequent need for ^{68}Ge source replacement. The convenience of obtaining transmission scans through CT fundamentally changed how PET would be typically performed in clinical practice.[42] CT, through extensive evaluation and validation, can be converted to a map of linear attenuation coefficients of the scanned object calibrated for 511 keV photons. This attenuation map can then be used for attenuation correction as well as scatter correction through anatomical models.

The advent of co-planar PET/MR brought a lot of promise for cardiac PET imaging because both cardiac PET and cardiac MR are highly sought-after advanced imaging modalities that may potentially offer complementary information in evaluating myocardial ischemia. As of today, there is no clearly established clinical indication for using this hybrid imaging modality though. Quantitatively, adding MR to PET (or adding PET to MR) in an integrated system would reverse the progress of using CT for PET attenuation and scatter corrections. However, solutions to use MR images and derived information for PET attenuation correction have been developed and are being evaluated at this time.[43–50]

It is important to note that not all technological advances for PET are widely available at this time because development is still ongoing. Different generations of PET scanners are being used on a daily basis. Depending on what is available, the most optimal imaging technique may vary. Special attention and considerations are needed to develop and standardize an optimal imaging protocol for quantitative cardiac PET, specifically focusing on high count rate capability, high sensitivity or low injected activity, and time-of-flight (TOF) acquisition capabilities that make the overall image quality better and produce less motion-related issues.

Attenuation and scatter corrections

First, it should be noted that attenuation and scatter corrections are significant in general PET imaging when quantitative accuracy, particularly activity concentration (in the unit of Bq/ml), is required. Accurate activity concentration in PET images is the first step towards any quantitative metrics used for static PET imaging (e.g. standardized uptake value (SUV)). In quantitative cardiac PET, quantitative accuracy is particularly important for assessing the pseudo-uniform perfusion deficit caused by multivessel coronary disease.[51]

Iterative image reconstruction algorithms take attenuation map and calculated scatter correction factors for quantitatively accurate 3D image creation. There are several technologies to generate an accurate attenuation map, including but not limited to external radioactive transmission sources, CT, and MRI. Machine learning based approaches have been also extensively applied to achieve this goal.[52,53] We will describe several examples of machine learning approaches in a later section.

Gating and motion compensation

Cardiac cycle, breathing as well as other voluntary and involuntary motions significantly affect the quantitative aspect of cardiac PET. Motion compensation techniques using electrocardiogram (ECG) and respiratory gating are generally more important in cardiac PET than in any other parts of the body because there are two involuntary motion fields (beating heart and respiration) that continue to influence the emission data. Since motion is often accounted for during the reconstruction and post-reconstruction processes, we will describe techniques and examples of motion compensation in a separate section below.

PET/CT

PET/CT makes quantitative aspects most streamlined assuming that CT images of the PET field-of-view are aligned accurately with PET emission data, allowing accurate attenuation and scatter correction. Manual and semi-automatic misalignment corrections are generally available in clinical software that perform post-processing of cardiac PET data. CT, in addition to replacing external radioactive transmission sources (e.g., ^{68}Ga rods), provides excellent anatomical details. If contrast-enhanced CT is acquired in a CT angiography (CTA) protocol, CT can also complement PET MPI as a one-stop imaging technology for anatomical assessment of coronary arteries as well as functional assessment of myocardial ischemia.

PET/MR

In cardiac PET/MR, MR is acquired simultaneously or sequentially using the same patient table. Cardiac MR, with its cardiac-specific protocol such as late gadolinium enhancement (LGE), could be obtained to assess myocardial tissue viability,[54–56] which are complementary to PET MPI. Quantitative cardiac PET still requires accurate attenuation and scatter corrections with motion corrections incorporated. Anatomical information from structural MRI has been extensively studied to acquire appropriate attenuation and scatter corrections in PET/MR ever since PET/MR was introduced in clinical practice. In general, the accuracy of attenuation and scatter with structural MRI are considered acceptable or arguably sufficient. Specifically for PET MPI, it may need more cardiac-specific validations and evaluations with perfusion imaging agents – which have not been extensively studied or counter-validated.[57]

Time-of-flight acquisition capability

Time-of-flight (TOF) PET detector technologies have become the industry standard for emission data acquisition in PET/CT. For PET/MR, TOF-PET is only partially incorporated since not all major vendors opted to choose TOF-capable PET detectors when PET/MR scanners were initially introduced.[58,59] Time-of-flight in PET imaging is related to how coincidence 511 keV photons are recorded by PET detectors. The two 511 keV photons from a positron-electron annihilation arrive at the two paired detectors to record a coincidence at slightly different times unless the annihilation occurs exactly at the center between the line of these two paired detectors. Until recently, commercial PET detector technologies ignored this slight difference in determining the coincidence. As PET detector technologies matured over time, it became technically feasible to record the time-of-flight (i.e., the time for each individual photon to arrive the detector) to determine the coincidence within a certain tolerance (i.e., coincidence timing resolution), typically in the range of a few hundred picoseconds. By incorporating TOF with this tolerance measured during data acquisition, iterative reconstruction algorithms used for PET image formation could record the location of this annihilation with a certain tolerance associated with the coincidence timing resolution. The importance of TOF-PET is undoubtable in state-of-the-art PET scanners, backed by enormous research and development efforts to improve the TOF-PET technologies.

Quantitative PET MPI can certainly benefit from TOF-PET. When coincidence timing resolution (CTR) of TOF-PET is improved, motion is better controlled in image reconstruction steps.[60] Furthermore, another benefit of improved contrast-to-background ratio from TOF-PET image reconstruction is improved automated segmentation of myocardium by clinical software, which in turn can be used to quantify regional and segmental myocardial flows. It is important to note that CTR performance is not the same among different TOF-PET scanners. The exact impact of TOF-PET on image segmentation is not fully evaluated. Therefore, this presumed benefit from TOF-PET should be more rigorously studied through realistic simulations, phantom measurements, and clinical image assessments to objectively assess the benefit of TOF-PET in cardiac PET imaging.

Dedicated cardiac PET

Unlike dedicated cardiac SPECT systems, dedicated cardiac PET systems are not widely available in the field. Exploration and research efforts of developing dedicated cardiac PET systems have been at best sporadic.[61,62] There are several reasons that commercial dedicated cardiac PET scanners have had little traction. Most can likely be attributed to the logistical complexity of running cardiac PET imaging facilities, which usually require, at minimum, a stress testing set up, a cyclotron or a $^{82}Sr/^{82}Rb$ generator, and cardiac-competent nursing staff members. However, it is not impossible to imagine a small private office offering a cardiac PET imaging program using a small footprint dedicated cardiac PET system. A $^{82}Sr/^{82}Rb$ generator or ^{18}F-based radiopharmaceuticals can be easily purchased and delivered from a local commercial radiopharmacy.

Dedicated cardiac PET systems, without CT or external radioactive transmission source for attenuation and scatter correction purposes, could suffer insufficient quantitative accuracy though. Expectation of better performance by allowing a smaller ring size that improves the nonlinear angulation problem of paired 511 keV photon detections for an improved spatial resolution, should be realized. Also, the benefit of TOF-PET should be carefully studied for small volume imaging like myocardial perfusion imaging to realize a high-performance dedicated cardiac PET scanner. Attenuation and scatter corrections using novel methods such as machine learning could also be a potential area for research and may improve the quantitative performance of a dedicated cardiac PET system.

Total-body PET/CT

Total-body PET/CT, also known as extremely long axial field of view (FOV) PET/CT, that covers all or most of the human body simultaneously is the latest entry to the PET technology development.[63–66] The benefit from the huge gain in system sensitivity for quantitative cardiac PET needs to be carefully evaluated. The most straightforward benefits are very low radiation dose as well as very high temporal resolution PET imaging that may alleviate the need for cardiac or respiratory gating (Fig. 6).[67]

One of known challenges for dynamic PET on the total-body PET/CT is choosing the radiopharmaceutical injection site. Intravenous (IV) injection of radiopharmaceutical is challenging while the patient lies on the PET/CT table because of the long length of the PET cylinder. Traditionally, radiopharmaceuticals were injected via an intravenous catheter located in the arm; however, IV access in the arm is very challenging for total-body PET/CT systems. An alternative location for IV access in dynamic total-body PET includes the legs.[67] In fact, by placing the IV line outside of the upper torso, one could avoid overlaying the IV line near the chest, avoiding errors in dynamic cardiac PET image analysis.

For quantitation, it is also important to develop an automated motion-resolved PET reconstruction algorithm to take advantage of the high temporal resolution. This could be revolutionary in terms of achieving high resolution and definition, potentially allowing more refined structural and voxel-by-voxel investigation of perfusion in the myocardium without any external gating device or breath-hold.

PET image reconstruction for myocardial perfusion imaging

Image reconstruction for PET data has seen extensive improvements in recent years. In particular, point-spread-function modeling, time-of-flight (TOF) photon detection,[68,69] regularized reconstruction,[70–73] and now deep learning-based approaches[74,75] have become areas of great interest in the field. Direct list-mode reconstruction algorithms are also of interest as they speed up the reconstruction time of dynamic multiframe reconstruction. Data acquired from TOF-PET benefit clearly improves reconstruction qualities and also impacts quantitative accuracy of the images.

Gating and motion compensation

ECG and respiratory gatings can be conducted with external devices. ECG-gating is now part of standard cardiac PET imaging. However, respiratory gating has not been standard for cardiac PET yet. The effect of respiratory motion is actually quite significant, causing nonnegligible blur, practically degrading image spatial resolution.[76]

Dual-gating of ECG and respiration further complicates the image quality. Conventional iterative image reconstruction results in reduced signal-to-noise ratio for gated bins that basically only consist of a fraction of the whole emission data. The more gated bins are used, the less photons detected in each gated bin are used for reconstruction, resulting in higher levels of noise.

Both cardiac and respiratory motions have nonnegligible effect on blurring in images reconstructed only using ECG-gated data. Because of blurring, the image spatial resolution for cardiac PET is usually much poorer than that of comparable images reconstructed using emission data that do not suffer much motion. Latest technological efforts to improve image contrast include incorporating motion fields to ECG-gated reconstruction to use 100% of the data in all cardiac bins and incorporating respiratory motion fields to further sharpen the reconstructed images, approaching the similar spatial resolution of reconstructed images using stationary emission data (Fig. 5).[77]

Direct list-mode reconstruction

Direct list-mode reconstruction algorithms also help greatly for gated and dynamic reconstructions. Processing the list-mode data as a whole and breaking up the gated bins and dynamic frames as part of reconstruction steps eliminate the need to create individual frames before reconstruction starts.

In addition, another direct approach could be performed when parametric images are of interest. In quantitative cardiac PET imaging, if the data are acquired dynamically, direct reconstruction of K_1, which is proportional to myocardial flow by the extraction fraction formula,[78] could help to get the images represented by physiologic parameters like MBF, instead of pixel intensity this way.

Dynamic PET and kinetic modeling

Dynamic cardiac PET, as well as SPECT, is essential to illustrate the tracer kinetics over time. In order to model the tracer kinetics and derive the influx rate constant of the radiopharmaceutical's extraction from the blood plasma to myocardial tissue and myocardial blood flow values, it is essential that dynamic imaging starts immediately once the radiopharmaceutical is administered. Dynamic cardiac PET does not always mean that the data acquisition is performed dynamically. Although prospective dynamic frames and data acquisition into pre-defined dynamic frames can be performed on some existing PET scanners, most of the modern PET scanners acquire the emission data only in list-mode. The list-mode data are the listing of each bit of the data that contain spatial, temporal, and other signals like ECG triggers and respiratory triggers from external devices into one big chunk of data file. This one data file is acquired for a pre-defined time, and once the data acquisition and radiopharmaceutical administration are synchronized, the acquired list-mode data are reconstructed into dynamic multiframes either directly or indirectly after de-listing of the list-mode data.

Specifically for this reason, reconstruction strategies, as discussed earlier, could be categorized into two different types: Direct reconstruction from the list-mode data, and traditional frame-by-frame reconstruction. Both reconstruction types provide the same dynamic data for kinetic modeling. These dynamic multiframe data are fed into the software that automates most of the calculations needed for kinetic modeling. Because of the nature of the kinetic modeling data processing, a few manual inputs and interventions are normal. Dynamic cardiac imaging for cardiac SPECT is also possible with new technologies and algorithms; however, quantification of radionuclide MPI such as MBF and CFR is more commonly performed using dynamic cardiac PET. When the kinetic model is incorporated as an intermediate reconstruction step, direct list-mode reconstruction of (kinetic) parametric images can be implemented.

PET kinetic modeling relies on tissue compartment model. Either one-tissue or two-tissue compartment model is used for dynamic cardiac PET. K_1, the rate constant from the blood plasma to tissue is calculated using a series of differential equations that govern tissue compartment models. The myocardial blood flow is basically identical to K_1 if the radiopharmaceutical or contrast agent modeled is freely diffusible and not metabolized into intracellular space. The only PET radiopharmaceutical for MPI that meets these conditions is ^{15}O-water. For other PET perfusion radiopharmaceuticals, once K_1 is calculated, the extraction fraction formula (as in Table 1) is applied to derive MBF. Since ^{15}O-water and ^{13}N-ammonia were extensively studied for cardiac PET, other radiopharmaceutical's extraction fraction formulas can be derived by comparing the K_1 values and incorporating physiologic models between the two radiopharmaceuticals' tracer kinetics obtained from the same subjects. All of the radiopharmaceuticals we described earlier have the extraction fraction formulas well established, enabling quantitative cardiac PET imaging as long as the software that incorporates the established formulas is available. Since several user inputs are often required, robustness depends on reproducibility of the automated and manual steps of the software as well as standardized dynamic multiframe time durations suitable for each radiopharmaceutical. Consistency in radiopharmaceutical administration (e.g., fast bolus,

slow bolus, etc.) and synchronization of radiopharmaceutical administration and data acquisition start time are other important factors for reproducible and robust quantitative PET MPI.[31,32]

The regional analysis for both MBF and CFR is characterized by segmental analysis often using 17-segments developed by the American Heart Association (AHA) or other established segments. Voxel-by-voxel analysis is also possible, and its precision is enhanced by excellent image spatial resolution that can be achieved through modern technological breakthroughs.

Another important challenge to calculate MBF and CFR using kinetic modeling is the accuracy of arterial input function (AIF) for tissue compartment models. The arterial input function in PET MPI is obtained from the dynamic multiframes of reconstructed images with volume of interests (VOIs) placed in left ventricular (LV) chamber or left atrial (LA) chamber. However, the motion and blurring causing spill-in and spill-out problems of partial volume effect make the derivation of AIF from LV or LA chambers subjective.[79] The clinically accepted software pays extra attention to placing these VOIs well within the blood pool chamber to minimize the partial volume effect, assuming motion is either resolved from reconstruction or blurring is already considered for deriving AIF.

Errors from inaccurate MBF calculations propagate to inaccurate CFR calculations. Since CFR calculations rely on MBFs of both stress and rest states, the error from MBF calculation is multiplicative in CFR calculation. Extra care is needed to minimize errors and to ensure reproducibility in MBF calculations.

Quantification parameters – MBF, CFR and their utilities

The utility of MBF and CFR from dynamic PET MPI has been shown in several clinical applications.[80–82] For example, absolute quantification in terms of MBF using ^{15}O-water cardiac PET showed that it was superior in the interpretation of myocardial perfusion, particularly in the interpretation of multivessel disease, when compared directly to standard relative perfusion images.[80] In another example, pharmacological stress MBF parametric images outperformed summed stress images in the task of detecting coronary artery disease (CAD).[81] The coronary flow reserve measured by ^{13}N-ammonia PET also showed its superior performance of detecting CAD over the performance of standard PET MPI.[82] Stress MBF or rest MBF individually could be valuable in selected populations. Stress MBF alone showed its role of detecting CAD[81,83] and was a potent outcome predictor of hypertrophic cardiomyopathy (HCM).[84] Elevated rest MBF was observed in patients with orthotopic heart transplantation,[85] and abnormal rest MBF was associated with major adverse cardiovascular outcomes such as unstable angina, non-ST and ST-elevation myocardial infarction, and stroke.[86]

Also, due to the nature of tissue compartment models, absolute quantification like MBF in a physical unit of flow (min^{-1}) does not depend on accurate measurement of administrated activity because activity values are all cancelled out during kinetic modeling computation. Multivessel coronary disease can be easily captured from MBF quantification since the

physical threshold of MBF can be established to determine normal vs. abnormal. Figure 7 shows this example clearly. When ^{15}O-water PET was quantified for MBF, multivessel disease, confirmed by invasive coronary angiography, is visually and numerically distinguished.

If cardiac PET imaging is performed to capture static distribution of perfusion, stress imaging can be performed either physically on a treadmill or pharmacologically using a vasodilator. However, if the cardiac PET imaging is performed to quantify MBF, the requirement of dynamic imaging to capture the tracer kinetics prohibits the use of physical stress testing, so that stress imaging should rely on pharmacological stress. There are multiple options for pharmacologic stress agents such as dipyridamole, regadenoson, and adenosine. All of these agents have been used in cardiac stress PET imaging. Although they are not the same, all of them seem to achieve enough stress conditions to assess hyperemic myocardial perfusion.

Cardiac PET combined with cardiac CT or cardiac MR

In addition to attenuation and scatter correction convenience, roles of CT angiography (CTA) or cardiac MR (CMR) are complementary to cardiac PET. CTA and CMR, as well as PET MPI, are all independently useful imaging modalities for assessing myocardial ischemia.[4]

With CTA, both functional perfusion information from PET MPI and structural information of coronary arteries from CTA can be comprehensively used for appropriate clinical intervention decisions. Calcium score, most commonly Agatston score that is based on the Hounsfield Unit provided by multidetector cardiac CT,[87] is another complementary information to PET MPI when PET/CT is performed.[88]

With CMR, cardiac PET/MR could also offer very comprehensive noninvasive assessment of myocardial ischemia. It is important to recognize the inherently different nature of MRI and PET. Late gadolinium enhancement is a reliable measure of tissue fibrosis. Given the exquisite sensitivity of the technique, it is able to detect different subendocardial degrees of necrosis. PET imaging counteracts the more limited resolution of the systems to detect fine subendocardial perfusion disbalances, with a more hemodynamic pattern of tissue response to the underlying vascular abnormalities. Technically, simultaneous CMR and dynamic PET MPI is challenging to implement, and an optimized protocol that includes logistical solutions for all components of dynamic PET MPI and CMR is needed.[89] Incorporating the need for dynamic cardiac PET using a fast-decaying radiopharmaceutical in the data acquisition workflow of cardiac PET/MRI is challenging, and the breath-hold acquisitions of common CMR sequences further complicate motion compensation for PET MPI data.

Role of machine learning in quantitative cardiac PET

Machine learning, specifically deep learning, has made significant waves in recent years for all imaging modalities including noninvasive cardiac imaging modalities. In general, machine learning approaches try to solve classification problems, and artificial intelligence of event prediction. Event prediction in image processing can reduce noise levels in final

images or intermediate data before final image generation. Since PET data are inherently signal-starved, noise in reconstructed images is a constant challenge.

Machine learning algorithms focusing on using retrospectively acquired datasets are often used to correlate the image data with disease diagnosis or outcomes. For example, outcome prediction using retrospective cardiac PET image data and subsequent cardiovascular events recorded could be performed using a deep learning technique.[90]

Noise reduction in PET images using deep learning, although not specific to cardiac PET, has been evaluated extensively.[91–93] Another area that deep learning has been investigated for PET is to apply attenuation and/or scatter corrections directly in image space[53,94] or indirectly[74,75] by creating pseudo-CT images that are converted to attenuation maps fed into image reconstruction steps. The deep learning method of attenuation and scatter corrections using only PET data is of great importance for dedicated small footprint PET technologies that do not have any transmission imaging capabilities.

Summary

The technology behind quantitative PET myocardial perfusion imaging that provides important and valuable quantification parameters such as MBF and CFR keeps evolving. The recent technological advances in PET such as much improved TOF-PET and extremely high-sensitivity long axial field of view PET as well as PET/CT and PET/MR are all highly relevant for quantitative PET MPI performance improvements. There are several radiopharmaceuticals appropriate for quantification of PET MPI. Of these radiopharmaceuticals, ^{82}Rb is widely available and ^{13}N-ammonia is likely the most validated radiopharmaceutical for quantification of MBF and CFR. Considering physical properties that relate to the highest quality PET image generation, ^{18}F-based radiopharmaceutical such as ^{18}F-flurpiridaz is of great interest as a next-generation PET MPI radiopharmaceutical, awaiting regulatory approvals. The quantification process involves kinetic modeling using tissue compartment models. For all radiopharmaceuticals studied for PET MPI, there have been a number of studies that showed procedures to perform appropriate kinetic modeling and validation of MBF generations. Implementation of these procedures require training of image quantification and establishing the analysis pipeline. It is important to understand that modern PET imaging technologies including TOF-PET, advanced motion compensation techniques, and machine learning approaches are not universally implemented. Clinical utilities of absolute quantification parameters like MBF and CFR have been shown in selected populations, and there have been an increasing number of reports in which MBF and CFR are used for detection of CAD and for prediction of cardiovascular events.

There are still important challenges to overcome for widespread use of quantitative PET MPI, including the logistical challenge of combining cardiac stress laboratory and advanced PET imaging expertise. With several appropriate radiopharmaceuticals available for PET MPI, it might be better if there is a single radiopharmaceutical as for ^{18}F-fluorodeoxyglucose (FDG) in most oncologic imaging, that can be widely distributed and provides excellent image quality and quantification. It will be also important to correctly and

appropriately implement advances in PET technology, which could result in lower radiation exposure, high spatial resolution, high signal-to-noise ratio, and quantification of MBF and CFR with high fidelity. Evidence of the utility of MBF and CFR in a broad spectrum of clinical applications will be key to enable more cardiac PET imaging centers to perform quantitative PET MPI instead of relying on conventional relative intensity-based image interpretation.

Acknowledgments

References

1. Fihn SD, Gardin JM, Abrams J, et al. 2012 ACCF/AHA/ACP/AATS/PCNA/SCAI/STS Guideline for the diagnosis and management of patients with stable ischemic heart disease: a report of the American College of Cardiology Foundation/American Heart Association Task Force on Practice Guidelines, and the American College of Physicians, American Association for Thoracic Surgery, Preventive Cardiovascular Nurses Association, Society for Cardiovascular Angiography and Interventions, and Society of Thoracic Surgeons. J Am Coll Cardiol. 2012;60:e44–e164. [PubMed: 23182125]

2. Joseph J, Velasco A, Hage FG, et al. Guidelines in review: Comparison of ESC and ACC/AHA guidelines for the diagnosis and management of patients with stable coronary artery disease. J Nucl Cardiol. 2018;25:509–515. [PubMed: 28884447]

3. Task Force M, Montalescot G, Sechtem U, et al. 2013 ESC guidelines on the management of stable coronary artery disease: the Task Force on the management of stable coronary artery disease of the European Society of Cardiology. Eur Heart J. 2013;34:2949–3003. [PubMed: 23996286]

4. Dewey M, Siebes M, Kachelriess M, et al. Clinical quantitative cardiac imaging for the assessment of myocardial ischaemia. Nat Rev Cardiol. 2020.

5. Ward RP, Al-Mallah MH, Grossman GB, et al. American Society of Nuclear Cardiology review of the ACCF/ASNC appropriateness criteria for single-photon emission computed tomography myocardial perfusion imaging (SPECT MPI). J Nucl Cardiol. 2007;14:e26–38. [PubMed: 18022098]

6. Al-Mallah MH, Sitek A, Moore SC, et al. Assessment of myocardial perfusion and function with PET and PET/CT. J Nucl Cardiol. 2010;17:498–513. [PubMed: 20379862]

7. Heydari B, Jerosch-Herold M, Kwong RY. Assessment of myocardial ischemia with cardiovascular magnetic resonance. Prog Cardiovasc Dis. 2011;54:191–203. [PubMed: 22014487]

8. Ramsey BC, Fentanes E, Choi AD, et al. Myocardial Assessment with Cardiac CT: Ischemic Heart Disease and Beyond. Curr Cardiovasc Imaging Rep. 2018;11:16. [PubMed: 29963220]

9. Maddahi J, Packard RR. Cardiac PET perfusion tracers: current status and future directions. Semin Nucl Med. 2014;44:333–343. [PubMed: 25234078]

10. Driessen RS, Raijmakers PG, Stuijfzand WJ, et al. Myocardial perfusion imaging with PET. Int J Cardiovasc Imaging. 2017;33:1021–1031. [PubMed: 28188475]

11. Conti M, Eriksson L. Physics of pure and non-pure positron emitters for PET: a review and a discussion. EJNMMI Phys. 2016;3:8. [PubMed: 27271304]

12. Nekolla SG, Reder S, Saraste A, et al. Evaluation of the novel myocardial perfusion positron-emission tomography tracer 18F-BMS-747158–02: comparison to 13N-ammonia and validation with microspheres in a pig model. Circulation. 2009;119:2333–2342. [PubMed: 19380625]

13. Fung EK, Carson RE. Cerebral blood flow with [15O]water PET studies using an image-derived input function and MR-defined carotid centerlines. Phys Med Biol. 2013;58:1903–1923. [PubMed: 23442733]

14. Lodge MA, Jacene HA, Pili R, et al. Reproducibility of tumor blood flow quantification with 15O-water PET. J Nucl Med. 2008;49:1620–1627. [PubMed: 18832120]

15. Herscovitch P, Markham J, Raichle ME. Brain blood flow measured with intravenous H2(15)O. I. Theory and error analysis. J Nucl Med. 1983;24:782–789. [PubMed: 6604139]

16. Wise RJ, Bernardi S, Frackowiak RS, et al. Measurement of regional cerebral blood flow, oxygen extraction ratio and oxygen utilization in stroke patients using positron emission tomography. Exp Brain Res. 1982;Suppl 5:182–186. [PubMed: 6983978]

17. Gould KL. PET perfusion imaging and nuclear cardiology. J Nucl Med. 1991;32:579–606. [PubMed: 2013799]

18. Karlish SJ, Stein WD. Passive rubidium fluxes mediated by Na-K-ATPase reconstituted into phospholipid vesicles when ATP- and phosphate-free. J Physiol. 1982;328:295–316. [PubMed: 6290646]

19. Sheehan RM, Renkin EM. Capillary, interstitial, and cell membrane barriers to blood-tissue transport of potassium and rubidium in mammalian skeletal muscle. Circ Res. 1972;30:588–607. [PubMed: 5026760]

20. Herrero P, Markham J, Shelton ME, et al. Noninvasive quantification of regional myocardial perfusion with rubidium-82 and positron emission tomography. Exploration of a mathematical model. Circulation. 1990;82:1377–1386. [PubMed: 2401071]

21. El Fakhri G, Kardan A, Sitek A, et al. Reproducibility and accuracy of quantitative myocardial blood flow assessment with (82)Rb PET: comparison with (13)N-ammonia PET. J Nucl Med. 2009;50:1062–1071. [PubMed: 19525467]

22. Ocneanu AF, deKemp RA, Renaud JM, et al. Optimally Repeatable Kinetic Model Variant for Myocardial Blood Flow Measurements with (82)Rb PET. Comput Math Methods Med. 2017;2017:6810626. [PubMed: 28293274]

23. Manabe O, Yoshinaga K, Katoh C, et al. Repeatability of rest and hyperemic myocardial blood flow measurements with 82Rb dynamic PET. J Nucl Med. 2009;50:68–71. [PubMed: 19091892]

24. Tahari AK, Lee A, Rajaram M, et al. Absolute myocardial flow quantification with (82)Rb PET/CT: comparison of different software packages and methods. Eur J Nucl Med Mol Imaging. 2014;41:126–135. [PubMed: 23982454]

25. DeGrado TR, Hanson MW, Turkington TG, et al. Estimation of myocardial blood flow for longitudinal studies with 13N-labeled ammonia and positron emission tomography. J Nucl Cardiol. 1996;3:494–507. [PubMed: 8989674]

26. Schelbert HR, Phelps ME, Huang SC, et al. N-13 ammonia as an indicator of myocardial blood flow. Circulation. 1981;63:1259–1272. [PubMed: 7226473]

27. Choi Y, Huang SC, Hawkins RA, et al. Quantification of myocardial blood flow using 13N-ammonia and PET: comparison of tracer models. J Nucl Med. 1999;40:1045–1055. [PubMed: 10452323]

28. Phelps ME, Hoffman EJ, Coleman RE, et al. Tomographic images of blood pool and perfusion in brain and heart. J Nucl Med. 1976;17:603–612. [PubMed: 818345]

29. Xiangsong Z, Dianchao Y, Anwu T. Dynamic 13N-ammonia PET: a new imaging method to diagnose hypopituitarism. J Nucl Med. 2005;46:44–47. [PubMed: 15632032]

30. Schepis T, Gaemperli O, Treyer V, et al. Absolute quantification of myocardial blood flow with 13N-ammonia and 3-dimensional PET. J Nucl Med. 2007;48:1783–1789. [PubMed: 17942816]

31. Yalcin H, Valenta I, Zhao M, et al. Comparison of two software systems for quantification of myocardial blood flow in patients with hypertrophic cardiomyopathy. J Nucl Cardiol. 2019;26:1243–1253. [PubMed: 29359273]

32. Monroy-Gonzalez AG, Juarez-Orozco LE, Han C, et al. Software reproducibility of myocardial blood flow and flow reserve quantification in ischemic heart disease: A (13)N-ammonia PET study. J Nucl Cardiol. 2019.

33. Chan SY, Brunken RC, Phelps ME, et al. Use of the metabolic tracer carbon-11-acetate for evaluation of regional myocardial perfusion. J Nucl Med. 1991;32:665–672. [PubMed: 2013805]

34. van den Hoff J, Burchert W, Borner AR, et al. [1-(11)C]Acetate as a quantitative perfusion tracer in myocardial PET. J Nucl Med. 2001;42:1174–1182. [PubMed: 11483676]

35. Armbrecht JJ, Buxton DB, Schelbert HR. Validation of [1–11C]acetate as a tracer for noninvasive assessment of oxidative metabolism with positron emission tomography in normal, ischemic, postischemic, and hyperemic canine myocardium. Circulation. 1990;81:1594–1605. [PubMed: 2110037]

36. Ahmed H, Haider A, Gisler L, et al. [(18) F]Flurpiridaz: Facile and Improved Precursor Synthesis for this Next-Generation Cardiac Positron Emission Tomography Imaging Agent. ChemMedChem. 2020.

37. Maddahi J, Bengel F, Czernin J, et al. Dosimetry, biodistribution, and safety of flurpiridaz F 18 in healthy subjects undergoing rest and exercise or pharmacological stress PET myocardial perfusion imaging. J Nucl Cardiol. 2019;26:2018–2030. [PubMed: 30488323]

38. Guehl NJ, Normandin MD, Wooten DW, et al. Single-scan rest/stress imaging: validation in a porcine model with (18)F-Flurpiridaz. Eur J Nucl Med Mol Imaging. 2017;44:1538–1546. [PubMed: 28365789]

39. Berman DS, Maddahi J, Tamarappoo BK, et al. Phase II safety and clinical comparison with single-photon emission computed tomography myocardial perfusion imaging for detection of coronary artery disease: flurpiridaz F 18 positron emission tomography. J Am Coll Cardiol. 2013;61:469–477. [PubMed: 23265345]

40. Berman DS, Germano G, Slomka PJ. Improvement in PET myocardial perfusion image quality and quantification with flurpiridaz F 18. J Nucl Cardiol. 2012;19 Suppl 1:S38–45. [PubMed: 22259005]

41. Sherif HM, Nekolla SG, Saraste A, et al. Simplified quantification of myocardial flow reserve with flurpiridaz F 18: validation with microspheres in a pig model. J Nucl Med. 2011;52:617–624. [PubMed: 21441533]

42. Beyer T, Townsend DW, Brun T, et al. A combined PET/CT scanner for clinical oncology. J Nucl Med. 2000;41:1369–1379. [PubMed: 10945530]

43. Catana C, van der Kouwe A, Benner T, et al. Toward implementing an MRI-based PET attenuation-correction method for neurologic studies on the MR-PET brain prototype. J Nucl Med. 2010;51:1431–1438. [PubMed: 20810759]

44. Hofmann M, Pichler B, Scholkopf B, et al. Towards quantitative PET/MRI: a review of MR-based attenuation correction techniques. Eur J Nucl Med Mol Imaging. 2009;36 Suppl 1:S93–104. [PubMed: 19104810]

45. Leynes AP, Yang J, Shanbhag DD, et al. Hybrid ZTE/Dixon MR-based attenuation correction for quantitative uptake estimation of pelvic lesions in PET/MRI. Med Phys. 2017;44:902–913. [PubMed: 28112410]

46. Monnier F, Fayad H, Bert J, et al. Generation of pseudo-CT from a single MRI for PET/MR attenuation correction purposes. EJNMMI Phys. 2014;1:A74. [PubMed: 26501665]

47. Teuho J, Saunavaara V, Tolvanen T, et al. Quantitative Evaluation of 2 Scatter-Correction Techniques for (18)F-FDG Brain PET/MRI in Regard to MR-Based Attenuation Correction. J Nucl Med. 2017;58:1691–1698. [PubMed: 28336781]

48. Vontobel J, Liga R, Possner M, et al. MR-based attenuation correction for cardiac FDG PET on a hybrid PET/MRI scanner: comparison with standard CT attenuation correction. Eur J Nucl Med Mol Imaging. 2015;42:1574–1580. [PubMed: 26091704]

49. Yang J, Jian Y, Tohme M, et al. Impact of atlas-CT-based bone anatomy compensation on MR-based attenuation correction for brain PET imaging in a time-of-flight PET/MRI system: A direct comparison to a patient-CT-based approach. EJNMMI Phys. 2015;2:A68. [PubMed: 26956328]

50. Yang X, Fei B. Multiscale segmentation of the skull in MR images for MRI-based attenuation correction of combined MR/PET. J Am Med Inform Assoc. 2013;20:1037–1045. [PubMed: 23761683]

51. Ziadi MC. Myocardial flow reserve (MFR) with positron emission tomography (PET)/computed tomography (CT): clinical impact in diagnosis and prognosis. Cardiovasc Diagn Ther. 2017;7:206–218. [PubMed: 28540215]

52. Arabi H, Bortolin K, Ginovart N, et al. Deep learning-guided joint attenuation and scatter correction in multitracer neuroimaging studies. Hum Brain Mapp. 2020.

53. Yang J, Park D, Gullberg GT, et al. Joint correction of attenuation and scatter in image space using deep convolutional neural networks for dedicated brain (18)F-FDG PET. Phys Med Biol. 2019;64:075019. [PubMed: 30743246]

54. Klein C, Gebker R, Kokocinski T, et al. Combined magnetic resonance coronary artery imaging, myocardial perfusion and late gadolinium enhancement in patients with suspected coronary artery disease. J Cardiovasc Magn Reson. 2008;10:45. [PubMed: 18928521]

55. von Spiczak J, Mannil M, Kozerke S, et al. 3D image fusion of whole-heart dynamic cardiac MR perfusion and late gadolinium enhancement: Intuitive delineation of myocardial hypoperfusion and scar. J Magn Reson Imaging. 2018;48:1129–1138. [PubMed: 29603482]

56. Yan AT, Gibson CM, Larose E, et al. Characterization of microvascular dysfunction after acute myocardial infarction by cardiovascular magnetic resonance first-pass perfusion and late gadolinium enhancement imaging. J Cardiovasc Magn Reson. 2006;8:831–837. [PubMed: 17060106]

57. Lassen ML, Rasul S, Beitzke D, et al. Assessment of attenuation correction for myocardial PET imaging using combined PET/MRI. J Nucl Cardiol. 2019;26:1107–1118. [PubMed: 29168158]

58. Muehlematter UJ, Nagel HW, Becker A, et al. Impact of time-of-flight PET on quantification accuracy and lesion detection in simultaneous (18)F-choline PET/MRI for prostate cancer. EJNMMI Res. 2018;8:41. [PubMed: 29855728]

59. Kero T, Nordstrom J, Harms HJ, et al. Quantitative myocardial blood flow imaging with integrated time-of-flight PET-MR. EJNMMI Phys. 2017;4:1. [PubMed: 28058674]

60. Vandenberghe S, Mikhaylova E, D'Hoe E, et al. Recent developments in time-of-flight PET. EJNMMI Phys. 2016;3:3. [PubMed: 26879863]

61. Oliver S, Moliner L, Ilisie V, et al. Simulation Study for Designing a Dedicated Cardiac TOF-PET System. Sensors (Basel). 2020;20.

62. Peng H Design study of a cardiac-dedicated PET system. Nuclear Instruments & Methods in Physics Research Section a-Accelerators Spectrometers Detectors and Associated Equipment. 2015;779:39–46.

63. Zhang YQ, Hu PC, Wu RZ, et al. The image quality, lesion detectability, and acquisition time of (18)F-FDG total-body PET/CT in oncological patients. Eur J Nucl Med Mol Imaging. 2020.

64. Badawi RD, Shi H, Hu P, et al. First Human Imaging Studies with the EXPLORER Total-Body PET Scanner. J Nucl Med. 2019;60:299–303. [PubMed: 30733314]

65. Leung EK, Judenhofer MS, Cherry SR, et al. Performance assessment of a software-based coincidence processor for the EXPLORER total-body PET scanner. Phys Med Biol. 2018;63:18NT01.

66. Zhang X, Zhou J, Cherry SR, et al. Quantitative image reconstruction for total-body PET imaging using the 2-meter long EXPLORER scanner. Phys Med Biol. 2017;62:2465–2485. [PubMed: 28240215]

67. Zhang XZ, Cherry SR, Xie ZH, et al. Subsecond total-body imaging using ultrasensitive positron emission tomography. Proceedings of the National Academy of Sciences of the United States of America. 2020;117:2265–2267. [PubMed: 31964808]

68. Presotto L, Gianolli L, Gilardi MC, et al. Evaluation of image reconstruction algorithms encompassing Time-Of-Flight and Point Spread Function modelling for quantitative cardiac PET: phantom studies. J Nucl Cardiol. 2015;22:351–363. [PubMed: 25367452]

69. Armstrong IS, Tonge CM, Arumugam P. Impact of point spread function modeling and time-of-flight on myocardial blood flow and myocardial flow reserve measurements for rubidium-82 cardiac PET. J Nucl Cardiol. 2014;21:467–474. [PubMed: 24477406]

70. Lindstrom E, Lindsjo L, Sundin A, et al. Evaluation of block-sequential regularized expectation maximization reconstruction of (68)Ga-DOTATOC, (18)F-fluoride, and (11)C-acetate whole-body examinations acquired on a digital time-of-flight PET/CT scanner. EJNMMI Phys. 2020;7:40. [PubMed: 32542512]

71. Seo Y, Khalighi MM, Wangerin KA, et al. Quantitative and Qualitative Improvement of Low-Count [(68)Ga]Citrate and [(90)Y]Microspheres PET Image Reconstructions Using Block Sequential Regularized Expectation Maximization Algorithm. Mol Imaging Biol. 2020;22:208–216. [PubMed: 30993558]

72. Ter Voert E, Muehlematter UJ, Delso G, et al. Quantitative performance and optimal regularization parameter in block sequential regularized expectation maximization reconstructions in clinical (68)Ga-PSMA PET/MR. EJNMMI Res. 2018;8:70. [PubMed: 30054750]

73. Tragardh E, Minarik D, Almquist H, et al. Impact of acquisition time and penalizing factor in a block-sequential regularized expectation maximization reconstruction algorithm on a Si-photomultiplier-based PET-CT system for (18)F-FDG. EJNMMI Res. 2019;9:64. [PubMed: 31342214]

74. Gong K, Yang J, Kim K, et al. Attenuation correction for brain PET imaging using deep neural network based on Dixon and ZTE MR images. Phys Med Biol. 2018;63:125011. [PubMed: 29790857]

75. Leynes AP, Yang J, Wiesinger F, et al. Zero-Echo-Time and Dixon Deep Pseudo-CT (ZeDD CT): Direct Generation of Pseudo-CT Images for Pelvic PET/MRI Attenuation Correction Using Deep Convolutional Neural Networks with Multiparametric MRI. J Nucl Med. 2018;59:852–858. [PubMed: 29084824]

76. Le Meunier L, Maass-Moreno R, Carrasquillo JA, et al. PET/CT imaging: Effect of respiratory motion on apparent myocardial uptake. Journal of Nuclear Cardiology. 2006;13:821–830. [PubMed: 17174813]

77. Slomka PJ, Rubeaux M, Le Meunier L, et al. Dual-Gated Motion-Frozen Cardiac PET with Flurpiridaz F 18. J Nucl Med. 2015;56:1876–1881. [PubMed: 26405171]

78. Shi L, Lu Y, Wu J, et al. Direct List Mode Parametric Reconstruction for Dynamic Cardiac SPECT. IEEE Trans Med Imaging. 2020;39:119–128. [PubMed: 31180845]

79. Vasquez AF, Johnson NP, Gould KL. Variation in quantitative myocardial perfusion due to arterial input selection. JACC Cardiovasc Imaging. 2013;6:559–568. [PubMed: 23582357]

80. Kajander SA, Joutsiniemi E, Saraste M, et al. Clinical value of absolute quantification of myocardial perfusion with (15)O-water in coronary artery disease. Circ Cardiovasc Imaging. 2011;4:678–684. [PubMed: 21926262]

81. Hajjiri MM, Leavitt MB, Zheng H, et al. Comparison of positron emission tomography measurement of adenosine-stimulated absolute myocardial blood flow versus relative myocardial tracer content for physiological assessment of coronary artery stenosis severity and location. JACC Cardiovasc Imaging. 2009;2:751–758. [PubMed: 19520347]

82. Fiechter M, Ghadri JR, Gebhard C, et al. Diagnostic value of 13N-ammonia myocardial perfusion PET: added value of myocardial flow reserve. J Nucl Med. 2012;53:1230–1234. [PubMed: 22776752]

83. Joutsiniemi E, Saraste A, Pietila M, et al. Absolute flow or myocardial flow reserve for the detection of significant coronary artery disease? Eur Heart J Cardiovasc Imaging. 2014;15:659–665. [PubMed: 24408930]

84. Castagnoli H, Ferrantini C, Coppini R, et al. Role of quantitative myocardial positron emission tomography for risk stratification in patients with hypertrophic cardiomyopathy: a 2016 reappraisal. Eur J Nucl Med Mol Imaging. 2016;43:2413–2422. [PubMed: 27527796]

85. Pampaloni MH, Shrestha UM, Sciammarella M, et al. Noninvasive PET quantitative myocardial blood flow with regadenoson for assessing cardiac allograft vasculopathy in orthotopic heart transplantation patients. J Nucl Cardiol. 2017;24:1134–1144. [PubMed: 28138813]

86. Guerraty MA, Rao HS, Anjan VY, et al. The role of resting myocardial blood flow and myocardial blood flow reserve as a predictor of major adverse cardiovascular outcomes. PLoS One. 2020;15:e0228931. [PubMed: 32053688]

87. Agatston AS, Janowitz WR, Hildner FJ, et al. Quantification of coronary artery calcium using ultrafast computed tomography. J Am Coll Cardiol. 1990;15:827–832. [PubMed: 2407762]

88. Pursnani A, Tawakol A. PET/CT imaging of myocardial blood flow and arterial calcium: Putting the pieces together. J Nucl Cardiol. 2013;20:331–333. [PubMed: 23512168]

89. Nensa F, Bamberg F, Rischpler C, et al. Hybrid cardiac imaging using PET/MRI: a joint position statement by the European Society of Cardiovascular Radiology (ESCR) and the European Association of Nuclear Medicine (EANM). Eur Radiol. 2018;28:4086–4101. [PubMed: 29717368]

90. Juarez-Orozco LE, Martinez-Manzanera O, van der Zant FM, et al. Deep Learning in Quantitative PET Myocardial Perfusion Imaging: A Study on Cardiovascular Event Prediction. JACC Cardiovasc Imaging. 2020;13:180–182. [PubMed: 31607660]

91. Liu CC, Qi J. Higher SNR PET image prediction using a deep learning model and MRI image. Phys Med Biol. 2019;64:115004. [PubMed: 30844784]

92. Kim K, Wu D, Gong K, et al. Penalized PET Reconstruction Using Deep Learning Prior and Local Linear Fitting. IEEE Trans Med Imaging. 2018;37:1478–1487. [PubMed: 29870375]

93. Haggstrom I, Schmidtlein CR, Campanella G, et al. DeepPET: A deep encoder-decoder network for directly solving the PET image reconstruction inverse problem. Medical Image Analysis. 2019;54:253–262. [PubMed: 30954852]

94. Shiri I, Arabi H, Geramifar P, et al. Deep-JASC: joint attenuation and scatter correction in whole-body (18)F-FDG PET using a deep residual network. Eur J Nucl Med Mol Imaging. 2020.

95. Di Carli MF, Dorbala S, Meserve J, et al. Clinical myocardial perfusion PET/CT. J Nucl Med. 2007;48:783–793. [PubMed: 17475968]
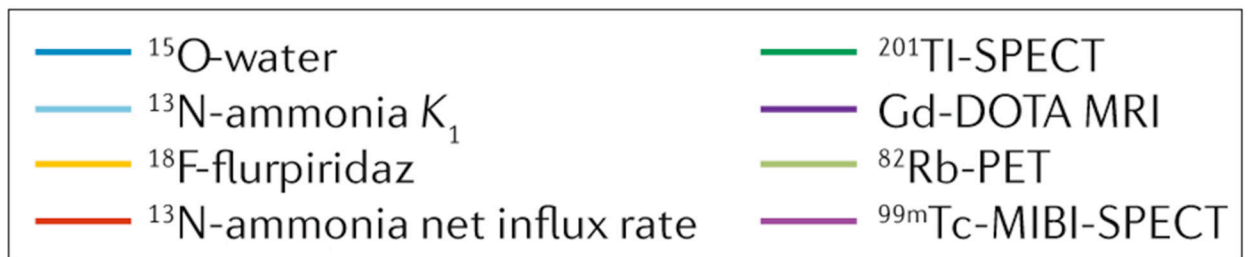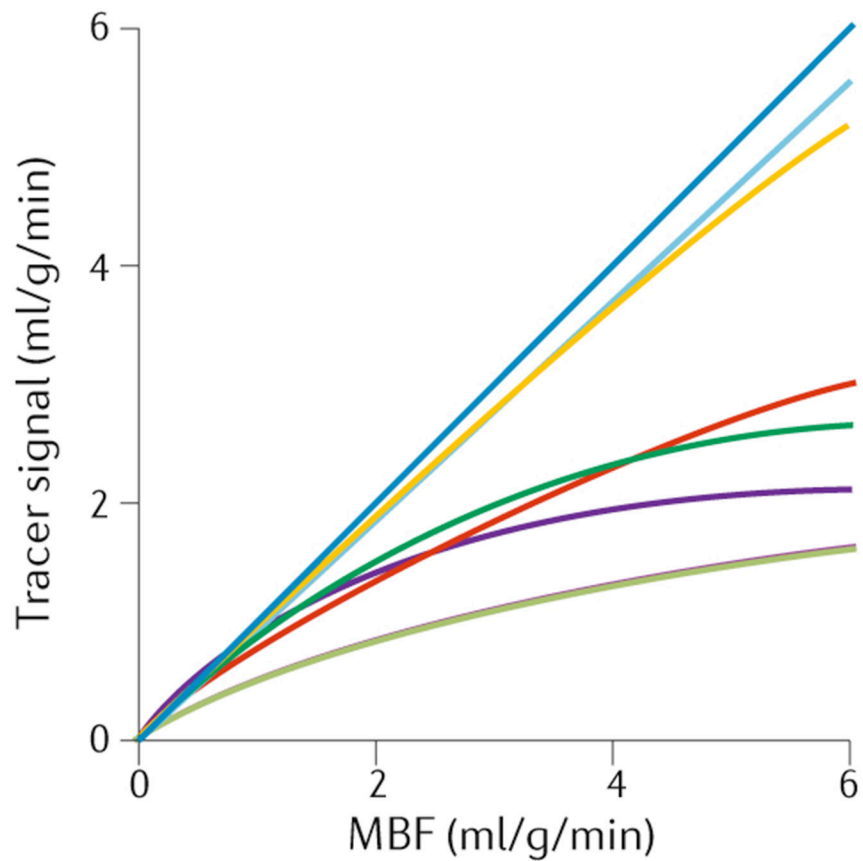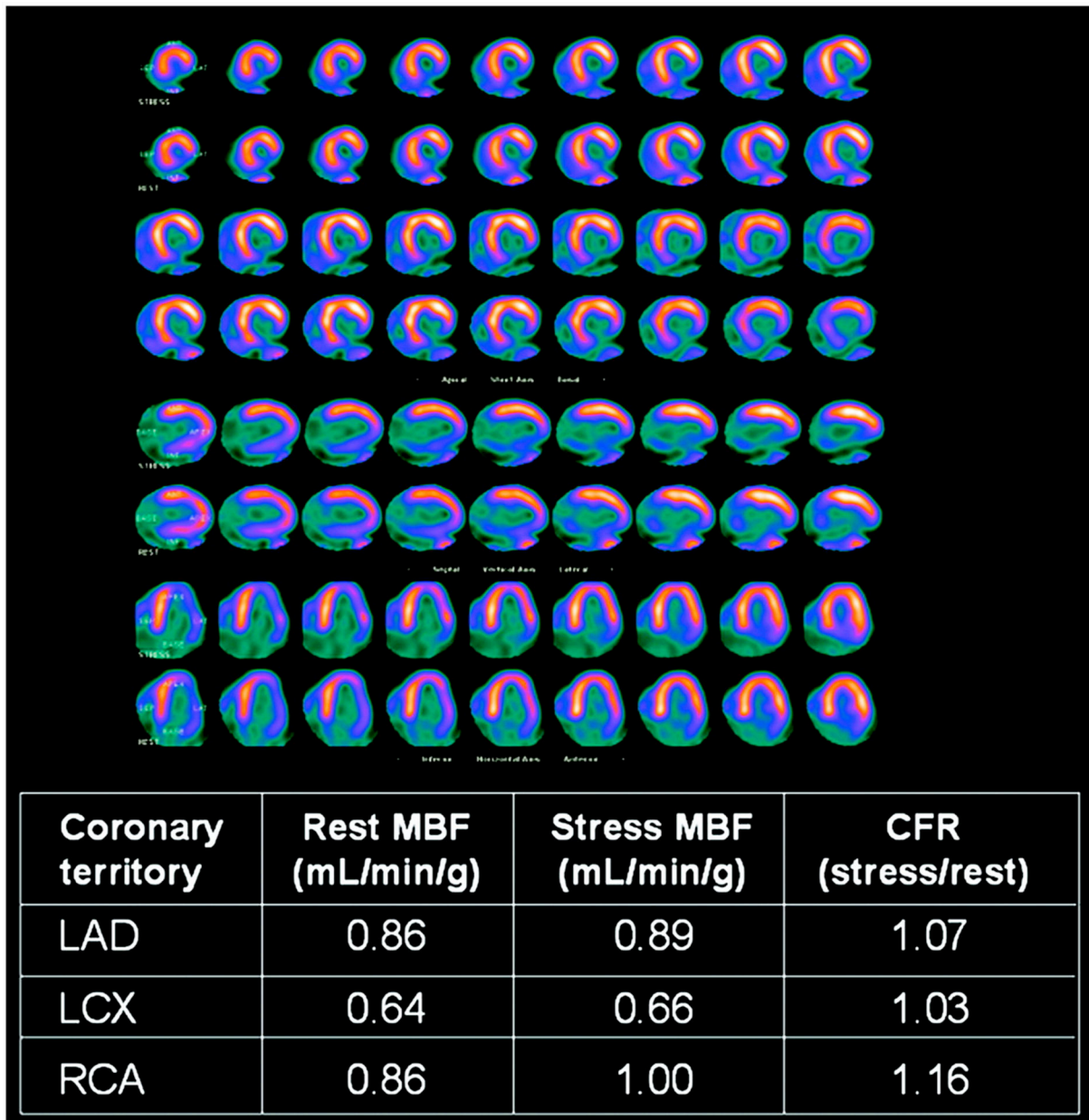
FIGURE 1.

Relationship between uptake (tracer signal) and myocardial blood flow for ^{15}O-water, ^{13}N-ammonia, ^{18}F-flurpiridaz, and other relevant radiopharmaceuticals for radionuclide-based myocardial perfusion imaging. This figure is adapted from Dewey M, et al.[4] under a Creative Commons Attribution 4.0 International License (http://creativecommons.org/licenses/by/4.0/).
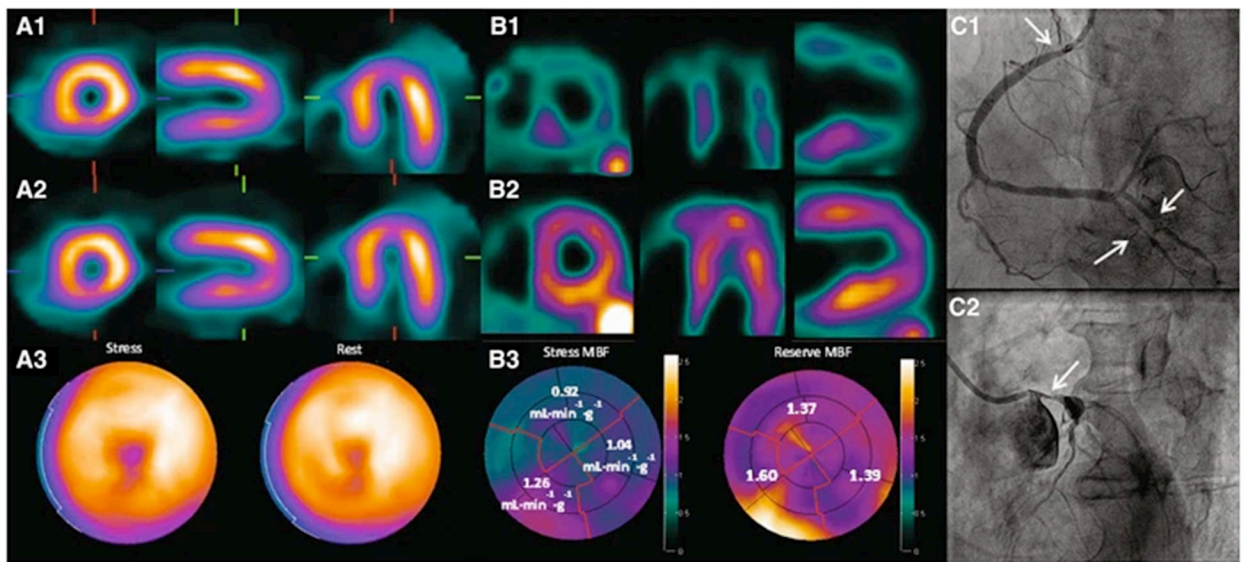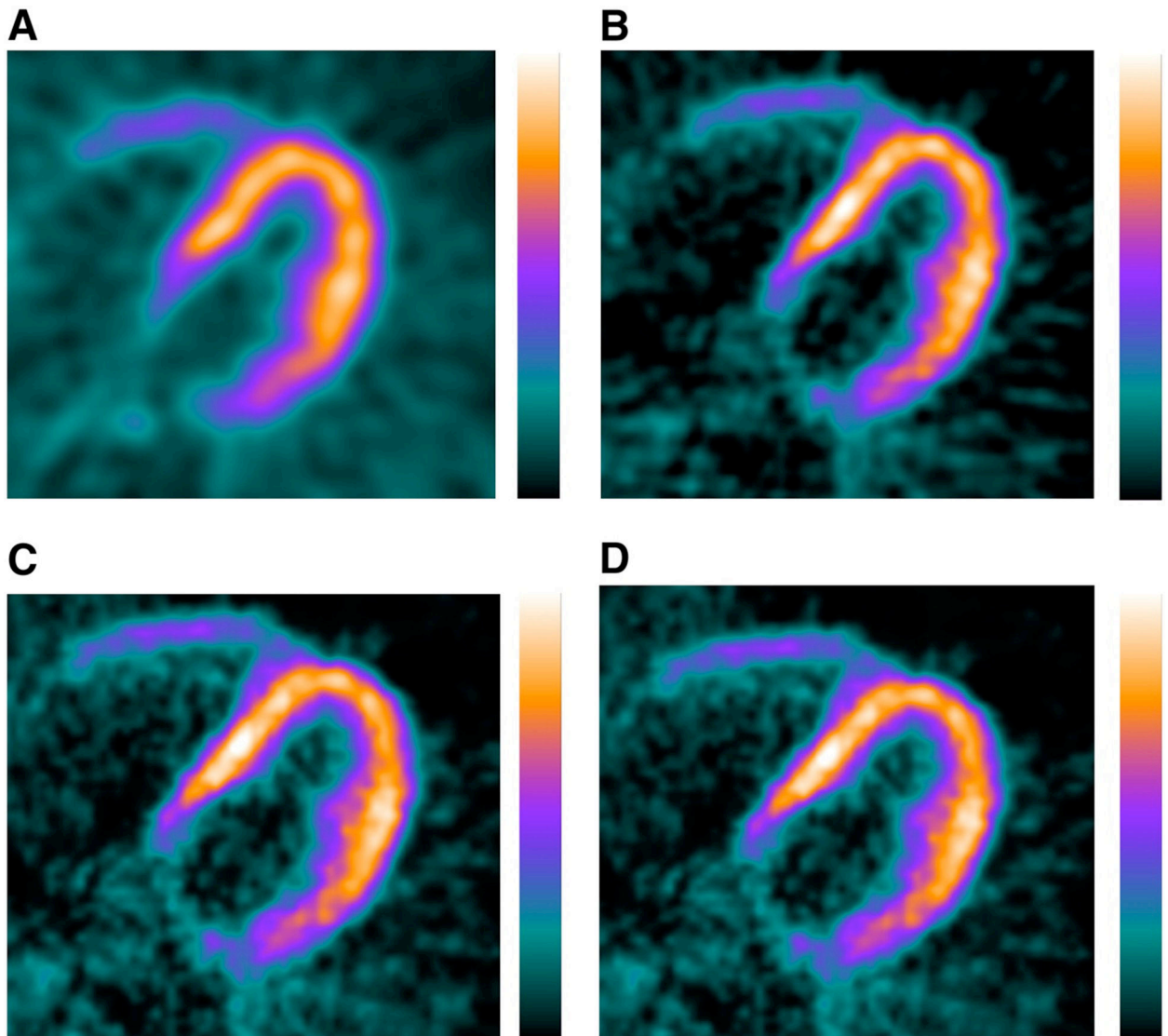
FIGURE 2.
Short and long axis slices of stress-rest ^{82}Rb-PET (top) and calculated MBF and CFR in three coronary artery territories (LAD: left anterior descending coronary artery; LCX: left circumflex coronary artery; RCA: right coronary artery). This figure was originally published in *JNM*. Di Carli MF, et al. Clinical Myocardial Perfusion PET/CT. J Nucl Med. 2007;48:783–793.[95] ©SNMMI.

Coronary territory	Rest MBF (mL/min/g)	Stress MBF (mL/min/g)	CFR (stress/rest)
LAD	0.86	0.89	1.07
LCX	0.64	0.66	1.03
RCA	0.86	1.00	1.16

FIGURE 3.

Transaxial images obtained from a representative patient using ^{13}N-ammonia PET. Images are from two different acquisition modes (2D - A and 3D – B, C, and D) with two different injected activities (900 MBq for 2D and 500 MBq for 3D). Different reconstruction algorithms show qualitative image quality differences. (A) 2D filtered backprojection (FBP), (B) 3D Fourier rebinning (FORE) FBP, (C) 3D FORE ordered subsets expectation maximization (OSEM), and (D) 3D reprojection (RP) algorithms were used. This figure was originally published in *JNM*. Schepis T, et al. Absolute Quantification of Myocardial Blood Flow with ^{13}N-Ammonia and 3-Dimensional PET. J Nucl Med. 2007;48:1783–1789.[30] ©SNMMI.
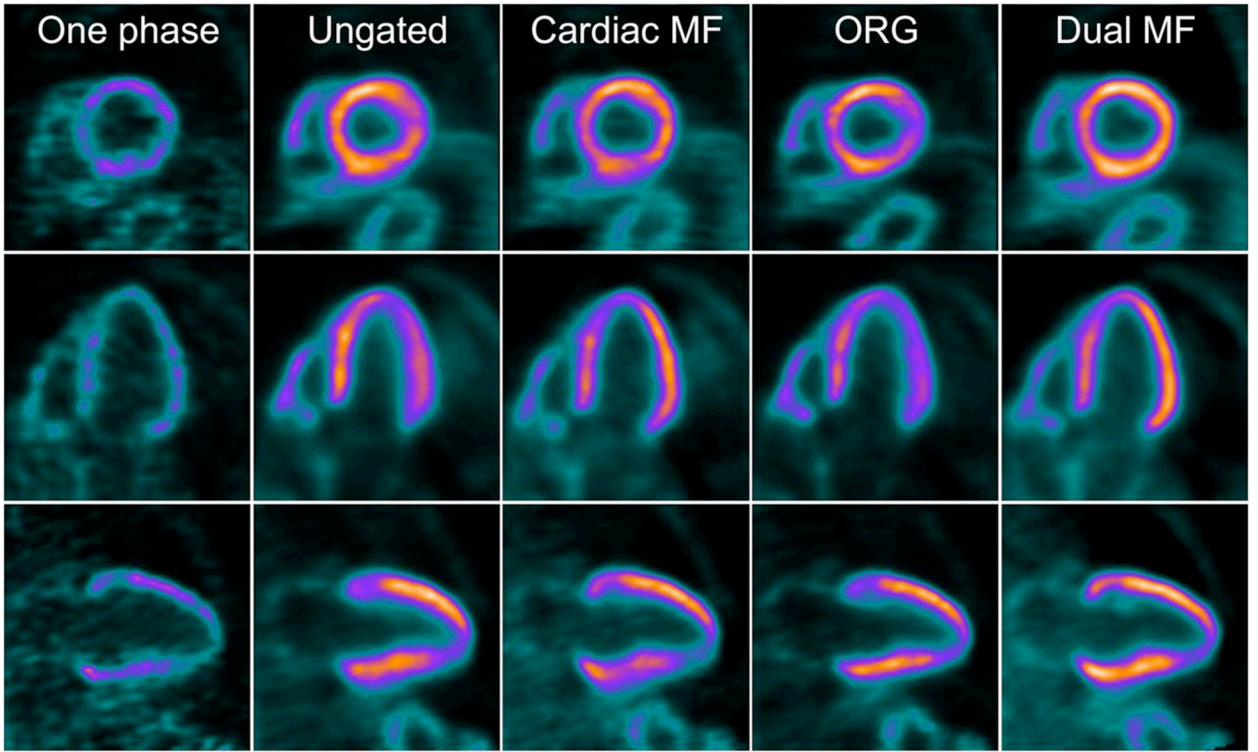
FIGURE 4.
Scatter histogram showing pixel-by-pixel correlation between MBF (f) calculated from ^{13}N-ammonia and K_1 calculated from ^{11}C-acetate. The sample size was 24 patients who underwent both ^{13}N-ammonia and ^{11}C-acetate PET MPI. This figure was originally published in *JNM*. Van den Hoff J, et al. [1-^{11}C]Acetate as a Quantitative Perfusion Tracer in Myocardial PET. J Nucl Med. 2001;42:1174–1182.[34] ©SNMMI.

$$K_1 = E \cdot f = (1 - 0.637\, e^{-1.198/f}) \cdot f$$
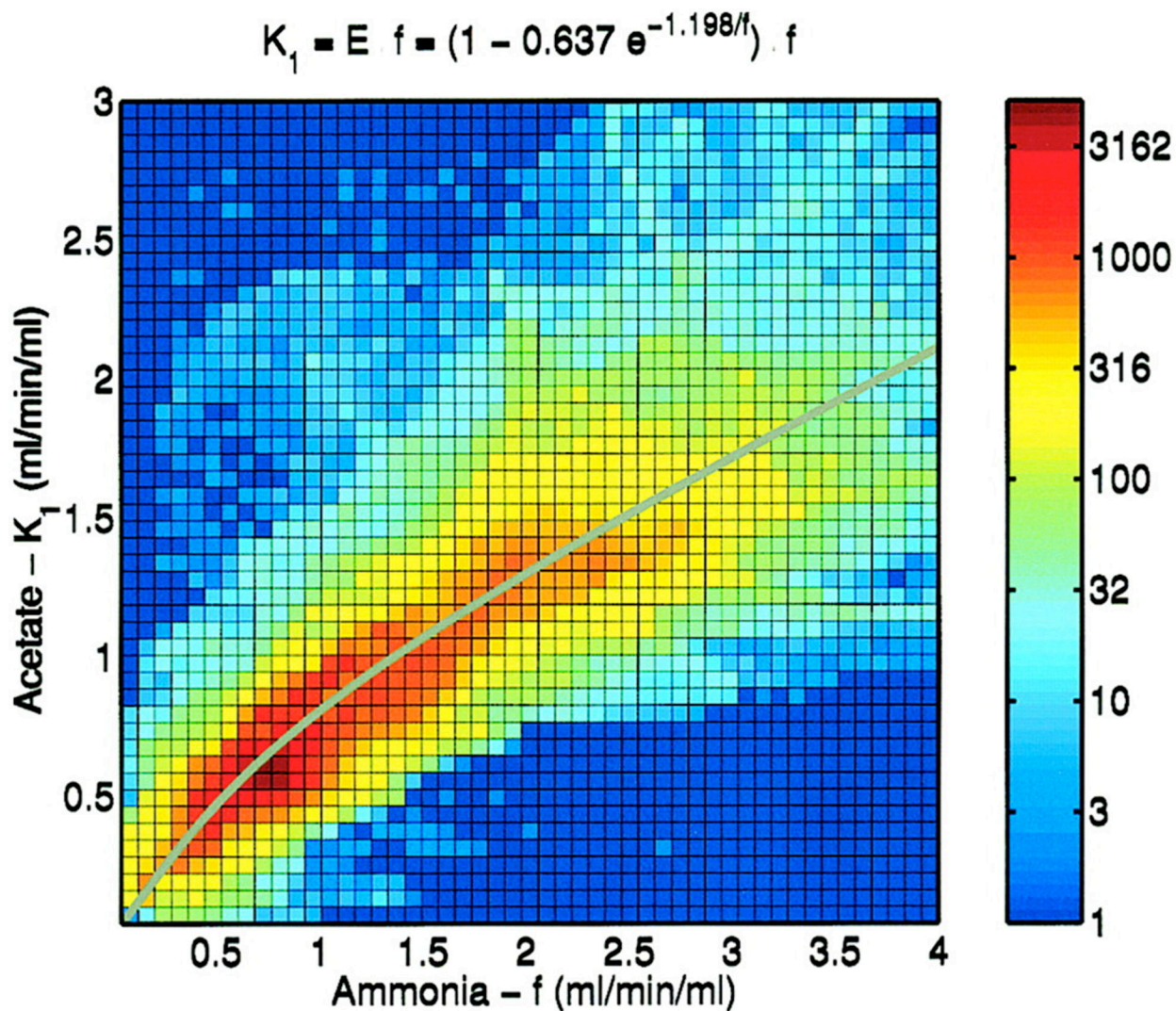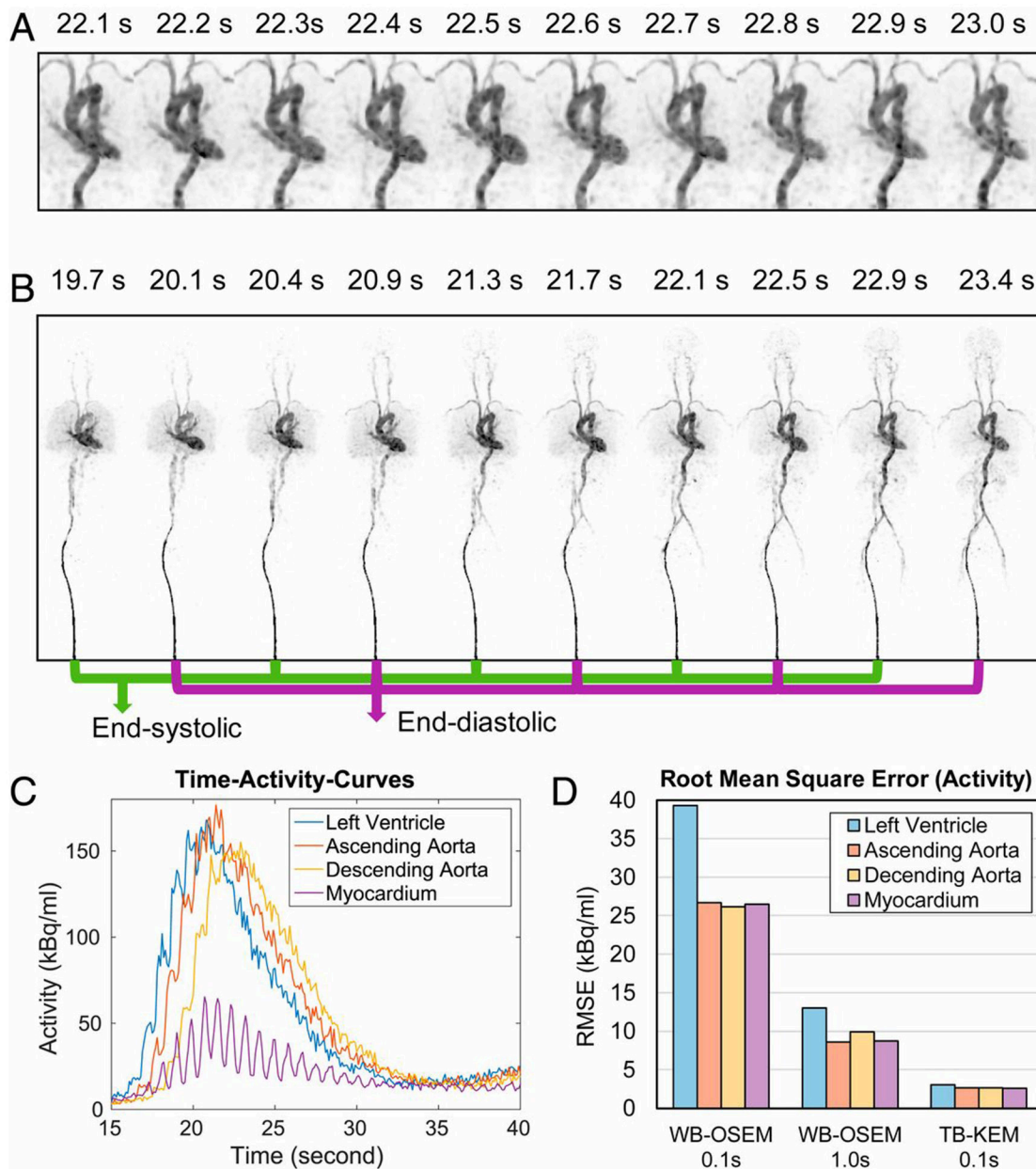

FIGURE 5.

Short- (top), vertical- (middle), and horizonal- (bottom) axis views of ^{18}F-flurpiridaz PET reconstructed using one cardiac phase, no gating summed (ungated), cardiac phases motion-frozen (all cardiac phases registered), optimal respiratory gating (ORG), and dual (cardiac and respiratory) phases motion-frozen (all cardiac and respiratory phases registered) data. This figure was originally published in *JNM*. Slomka PJ, et al. Dual-Gated Motion-Frozen Cardiac PET with Flurpiridaz F 18. J Nucl Med. 2015;56:1876–1881.[77] ©SNMMI.

FIGURE 6.
Reconstructed images (A and B) of dynamic ^{18}F-fluorodeoxyglucose PET obtained using uEXPLORER total-body PET, showing subsecond temporal resolution that captured very fine temporally resolved time-activity-curves (C) of arterial blood pool, and root-mean square error (RMSEs) of activities reconstituted from 0.1 s temporal resolutions of a conventional whole-body (WB)-OSEM reconstruction algorithm and the total-body kernel expectation maximization (KEM) algorithm, and 1.0 s temporal resolution of WB-OSEM. This figure is from Zhang X, et al.,[67] used under a Creative Commons Attribution-NonCommercial-NoDerivatives License 4.0 (CC BY-NC-ND) (http://creativecommons.org/licenses/by/4.0/).

FIGURE 7.

Short and long axis views and polar plots for [99mTc]-tetrofosmin SPECT (A1, A2, and A3) and [15O]-water PET (B1, B2, and B3), and x-ray angiography images (C1 and C2) showing multivessel coronary disease. This figure is from Driessen RS, et al.,[10] used under a Creative Commons Attribution 4.0 International License (http://creativecommons.org/licenses/by/4.0/).

TABLE 1.

Important properties of radiopharmaceuticals used in PET myocardial perfusion imaging. The physical half-life of the parent radionuclide (^{15}O, ^{82}Rb, ^{13}N, ^{11}C, and ^{18}F), mean positron range in water for the parent radionuclide (values are taken from[11]), and extraction (E) fraction formula that connects K_1 calculated from kinetic modeling and myocardial blood flow (MBF). $K_1 = \text{MBF} \cdot E$.

	Physical half-life of radionuclide (min)	Mean positron range in water (mm)	MBF & K_1 (mL min^{-1} g^{-1}) (extraction formula)
^{15}O-water	2.04	3.0	$K_1 = \text{MBF}$
^{82}Rb*	1.273	7.1	$K_1 = \text{MBF} \cdot (1 - e^{-(0.45 + 0.16\text{MBF})/\text{MBF}})$ for $0 \le \text{MBF} \le 0.92$; $\text{MBF} = 3.664 + (K_1 - 0.92)$ for $\text{MBF} > 0.92$ No relationship when $\text{MBF} > 3.7$
^{13}N-ammonia**	9.965	1.8	$K_1 = \text{MBF} \cdot E$
^{11}C-acetate***	20.334	1.2	$K_1 = \text{MBF} \cdot E$, or $K_1 = \text{MBF} \cdot (1 - 0.637e^{-1.198/\text{MBF}})$
^{18}F-flurpiridaz****	109.771	0.6	$K_1 = \text{MBF} \cdot 0.94$

*
There are slightly different expressions reported. The values in this table were taken from[21].

**
E is close to 1 for ^{13}N-ammonia. Either one-tissue compartment model or two-tissue compartment model is used to derive K_1.[25]

***
E is close to 1 for ^{11}C-acetate when the first-pass extraction data (i.e., first 2–3 minutes of dynamic data at most) are used. Using 2-tissue compartment model, a nonlinear extraction formula could be obtained as well.[34]

****
Although there is a roll-off of the linearity of the extraction fraction, the linearity is maintained at very high flow rates for ^{18}F-flurpiridaz.[12] For practical values of MBF, there is no need to correct for the nonlinearity.